

Scattering length of the ground state Mg+Mg collision.

E. Tiesinga, S. Kotochigova, and P. S. Julienne

Atomic Physics Division, NIST, 100 Bureau Drive Stop 8423, Gaithersburg, MD 20899-8423, USA.

Abstract

We have constructed the $X^1\Sigma_g^+$ potential for the collision between two ground state Mg atoms and analyzed the effect of uncertainties in the shape of the potential on scattering properties at ultra-cold temperatures. This potential reproduces the experimental term values to 0.2 cm^{-1} and has a scattering length of $+1.4(5)\text{ nm}$ where the error is predominantly due to the uncertainty in the dissociation energy and the C_6 dispersion coefficient. A positive sign of the scattering length suggests that a Bose-Einstein condensate of ground state Mg atoms is stable.

PACS numbers: 34.20.-b, 34.50.-s, 33.20.Vq, 31.15.Rh

I. INTRODUCTION

It was shown in Ref. [1] that Mg atoms can be magneto-optically trapped. This offers many possible applications of cold Mg atoms for ultra high resolution spectroscopy, new frequency standards and collective quantum effects. A magnesium clock has already been developed by Ref. [2]. The most abundant isotopes of Mg have a single electronic ground state without hyperfine interactions, which opens a road to simpler theoretical modeling of ground state atomic collisions as compared to the modeling of, say, alkali-metal atom collisions [3].

Magnesium is not the only alkaline earth species that can be magnetically and optically manipulated. Ingenious cooling schemes exist for Ca [4] and Sr [5–8]. For Sr Ref. [5] have nearly reached the quantum degeneracy regime. Optical clocks based on the ultra-cold calcium have been constructed for Mg [2] and Ca [9–13]. The first experimental photoassociation spectra were reported for calcium [14] while photoassociation spectroscopy for alkaline earth atoms has been studied theoretically in Ref. [15]

The coldest temperatures in dilute atomic gases are obtained by a process called evaporative cooling. Ground state collisions are crucial for evaporative cooling. Elastic collisions during this process lead to a thermalization of atoms and under the right conditions formation of a Bose condensate. Elastic collision rates at ultra cold temperatures can be described by a single parameter, the scattering length a . Formation of Bose-Einstein condensates is determined by the nonlinear coupling parameter in the condensate Schrödinger equation, which in turn depends on the sign and value of the scattering length.

Inelastic collisions, which change the internal state of the atoms, can eject trapped atoms. Examples of inelastic processes are, for example, spin-exchange, spin-depolarization, and Penning and associative ionization, where the first two have been observed in alkali-metal gases [3] and the latter have been observed in metastable rare gas samples [16]. For alkaline-earth atoms the electronic ground state is solely composed of closed shells and is a 1S_0 state. Consequently, no inelastic atom-atom collisions can occur. This opens a pathway to more efficient evaporative cooling.

In this paper we present our calculation of the ground state Mg_2 scattering length and cross-section as a function of the collision energy, using a potential constructed from high resolution spectra of the magnesium dimer measured by Balfour and Douglas [17]. At temperatures below 5 mK ground state Mg collisions are in the s-wave scattering regime and the $l = 0$ phase shift determines the cross-section and, at zero collision energy, the scattering length. This phase shift can be found by matching the numerically evaluated scattering wavefunction of the interaction potential to free scattering wavefunctions at large internuclear separation R . Slight changes to the inner part of the potential can generate significant changes in the phase shift and the scattering length.

We will discuss several ways to obtain the interaction potential of ground state Mg_2 . Firstly, a Rydberg-Klein-Rees (RKR) potential curve has been constructed in Ref. [17] from their measurement of the rovibrational levels ($\nu = 0 - 12$, $J = 10 - 76$) of ground state Mg_2 . Secondly, Vidal and Scheingraber [18] have reevaluated the molecular constants of Ref. [17] and improved upon the RKR analyses by applying a variational procedure based on the inverted perturbation approach (IPA). Finally, there exist a large number of theoretical electronic structure calculations [19–30] of the ground state Mg_2 potential. This paper

briefly describes our *ab initio* multiconfiguration valence bond (MVB) calculation of the ground state potential. Although, as we will show, the theoretical uncertainty in the shape of the potential is too large to predict the scattering length we nevertheless compare scattering data for our *ab initio* potential and the most recently published theoretical potential by Czuchaj *et al.* [30] to those for the RKR and IPA potential. This will give us a feeling for the state of the art in molecular electronic structure calculations of interacting two electron atoms.

This paper is set up as follows. In Section II we describe the existing experimental data and the potentials that have been constructed from the data. Section III presents the theoretical calculations in the existing literature as well as a new calculation using the multiconfiguration valence bond method. Section IV describes the long-range behavior of the potentials and connects this to the short-range potentials obtained in Sections II and III. Finally, Section V discusses how well bound states of the four potentials that have been constructed reproduce the experimental bound state energies, and determines the scattering properties for the best of these four potentials.

II. EXPERIMENTAL DATA AND THE GROUND STATE POTENTIAL

The RKR potential of Ref. [17] and the IPA potential constructed in this work from data published in Ref. [18] are shown in Fig. 1. For the RKR potential we use a dissociation energy $D_e = 424(5) \text{ cm}^{-1}$ ($1 \text{ cm}^{-1} = 29.9792458 \text{ GHz}$), defined as the energy difference between the bottom of the potential and the asymptotic energy. Reference [18] did not provide a tabulated IPA potential but expressed the potential in terms of Dunham coefficients Y_{lm} . We have constructed a potential from the Y_{lm} for $l = 0-3$, $m = 0-5$ provided in Table IV of Ref. [18] by applying the RKR procedure. We will call this potential the IPA potential. We will show later on by solving the Schrödinger equation for the RKR and IPA potentials that the IPA potential reproduces the term values significantly better than the RKR potential of Ref. [17]. For the IPA potential we take the dissociation energy D_e to be $431.0(1.0) \text{ cm}^{-1}$ in accordance with fit of Ref. [18] to the last outer turning points of the potential. The 1.0 cm^{-1} uncertainty is based on the sensitivity of the fit with the order of the long-range dispersion expansion. The RKR and IPA potential are only known over a limited region of internuclear separation, $6 a_0$ to $14 a_0$. This range is determined by the inner and outer turning point of the most-weakly-bound measured rovibrational level.

For a scattering calculation the potential must be known for all internuclear separations. Therefore we have connected the repulsive short range of the RKR potential to the repulsive wall of our MVB potential which will be discussed in Section III. The repulsive short range wall of the IPA potential is a linear extrapolation from the attractive region as our MVB potential could not be smoothly connected to the IPA potential. Both RKR and IPA potentials suffer from a well known “short range turnover” in the potential inherent to the RKR inversion procedure. We simply removed those inner turning points from the data set before extrapolation. The extrapolation of the RKR and IPA potential to longer R is discussed in Section IV.

III. THE AB INITIO GROUND STATE POTENTIALS

The ground state Mg_2 molecule is formed from two closed shell atoms, each of which is described by the configuration $1s^2 2s^2 2p^6 3s^2$. This might suggest that theoretical modelling will be easy. Instead, numerous computational efforts have proven the opposite. The first dramatic complication arises at the Hartree-Fock level, because it predicts a purely repulsive ground state potential. The binding of the magnesium dimer is created by the correlation energy only. There are inter- and intrashell correlations affecting the potential, that, apparently, have a strong dependence on internuclear separation. The question becomes how well a computational approach can incorporate these correlations. There are a large number of methods [19–30] which have been tested for the computation of the correlation corrections. In a pioneering publication Stevens and Krauss [23] calculated the ground state potential of Mg_2 using a nonrelativistic multiconfiguration self-consistent field method. Their work shows the importance of the ability to simultaneously incorporate both the long-range atomic and short-range molecular correlations. Many-body perturbation theory can provide an alternative to the configuration interaction approach to model correlation effects in the Mg_2 molecule. Double excitation type diagrams were applied by Purvis and Bartlett [24] to significantly improve the molecular binding energy.

In Ref. [30] a combination of a coupled-cluster method with single and double excitations and perturbative triple excitations is used to reach a good agreement with the RKR potential of Ref. [17]. The potential curve of Ref. [30] is shown in Fig. 1.

For this paper we have used the multiconfiguration valence bond (MVB) method to calculate the ground state Mg_2 potential. A detailed description of the computational approach is given in Ref. [31]. We create a nonorthogonal basis set from self-consistent Dirac-Fock atomic orbitals belonging to the $[1s^2] 2s^2 2p^6 3s^2$ configuration and additional Sturmian orbitals labeled 3p, 3d, 4s, 4p, 5s, and 5p. The closed shells $1s^2 + 1s^2$ form the core of the molecule and no excitations from $1s^2 + 1s^2$ will be allowed. The $2s^2$, $2p^6$ and $3s^2$ orbitals are valence orbitals and single and double excitations from these orbitals occur. Various covalent and ionic configurations are constructed by distributing electrons from the optimized valence orbitals in all allowed ways over the 3p, 3d, 4s, 4p, 5s, and 5p orbitals. In total, there are 1041 molecular configurations in our configuration interaction. We have performed two kinds of nonrelativistic calculations. The first kind is aimed at calculating the best possible short-range potential by first perturbatively estimating the correlation energy of each molecular configuration excited from the ground state configuration. If the estimate falls below a threshold this configuration is not included in the configuration interaction procedure. This truncation of the configurations is necessary because inclusion of all configurations in the configuration interaction procedure is not computationally possible. The second kind of calculation gives the best possible long-range potential by excluding ionic configurations and switching off the exchange interaction in the Hamiltonian in order to reduce the size of the matrix and to accelerate the calculation. The two calculations are connected between $13 a_0$ and $14 a_0$, because at these internuclear separations the difference between the total energy of the two kinds of calculations, and thus the exchange energy, is less than 5% of the binding energy. Figure 1 shows our ground state $^1\Sigma_g^+$ potential of Mg_2 . The dissociation energy is $D_e = 410 \text{ cm}^{-1}$.

IV. LONG-RANGE POTENTIALS

The long-range dispersion potential of the Mg_2 ground state has attracted considerable attention over the past few decades. Mg_2 was the first alkaline earth van der Waals molecule for which a high accuracy RKR potential was obtained and thus allowing a comparison with, or extraction of, the long-range potential. Stwalley [32,33] and Li and Stwalley [34] constructed a dispersion potential using the form $V(R) = D_0 - C_6/R^6 - C_8/R^8$ from the frequency-dependent atomic dipole polarizability and the RKR curve. The dipole-dipole dispersion coefficient C_6 was determined from the atomic polarizability while both D_0 , the energy difference between the $\nu = 0, J = 0$ rovibrational level and the asymptotic energy, and dipole-quadrupole dispersion coefficient C_8 were then obtained by fitting to the RKR curve minus the dipole-dipole dispersion contribution. They find $D_0 = 404.1(0.5) \text{ cm}^{-1}$, $C_6 = 683(35) \text{ a.u.}$ (1 a.u. = 1 Hartree a_0^6 , 1 Hartree = $4.359743 \times 10^{-18} \text{ J}$), and $C_8 = 38(8) \times 10^3 \text{ a.u.}$ (1 a.u. = 1 Hartree a_0^8). In Ref. [35] the C_6 dispersion coefficient has been calculated based on atomic coupled-cluster theory. The result of this calculation is $C_6 = 647.8 \text{ a.u.}$. Upper and lower bounds for the dispersion coefficients have been obtained in Ref. [36] using a Pade approximation to bound the atomic multipole polarizabilities. Their ranges are $C_6 = 630 \text{ a.u.} - 638 \text{ a.u.}$ and $C_8 = 41100 \text{ a.u.} - 43500 \text{ a.u.}$. In addition they estimated the dipole-octupole coefficient, C_{10} , to be between 2730000 a.u. and 3040000 a.u. (1 a.u. = 1 Hartree a_0^{10}). Recently, Porsev and Derevianko [37] have calculated the C_6 coefficient using accurate theoretical and experimental atomic data. Different contributions to the C_6 coefficient were obtained with different atomic relativistic many-body electronic structure methods. The dominant contribution to this coefficient was found by combining configuration interaction and many-body perturbation theory. The reported value of $C_6 = 627(12) \text{ a.u.}$ agrees quite well with the bounds of Ref. [36]. Finally, the dispersion coefficients can be evaluated from molecular electronic structure calculations. They are extracted by fitting to the long-range shape of the interaction potential. For example, the induced dipole-dipole dispersion coefficient of Ref. [30] is about a factor of 2 larger, while that of our MVB calculation is about 15% smaller, than that of Ref. [37].

The long-range behavior of the RKR and IPA potentials, the dispersion potential obtained from Ref. [37,36], and our MVB calculation are shown in Fig. 2. The full line with filled diamonds and full line are the RKR and IPA potentials, respectively. The dotted line of the MVB calculation smoothly connects to the RKR at $13.53 a_0$. Although this smooth connection is fortuitous, it suggests that the RKR potential be extrapolated by the MVB potential. On the other hand the long-range dispersion potential denoted by the dash-dotted line using the C_6 coefficient of Ref. [37] and $C_8 = 42300 \text{ a.u.}$ and $C_{10} = 2885000 \text{ a.u.}$ of Ref. [36] smoothly connects to the IPA potential. The C_6 coefficient of Ref. [30] leads to a too attractive long-range behavior as shown by the dashed curve in the figure.

For our study of scattering properties the spectroscopically derived RKR and IPA potentials are extrapolated to large internuclear separations R using the dispersion plus exchange form $V_{dis}(R) + V_{ex}(R)$, where $V_{dis}(R) = -\sum_{n=6,8,10} C_n/R^n$ and $V_{ex}(R) = B \times R^\alpha \times \exp(-\beta R)$. For $R > 13.53 a_0$, the largest turning point of the RKR potential, this potential is best extrapolated by the dispersion coefficients extracted from the MVB potential and the exchange potential of Ref. [38]. The exchange contribution is small but has been added for completeness sake. Other values for these coefficients do not seem to be consistent with the shape of

the RKR potential. The IPA potential ending at $R = 14.5 a_0$ is smoothly joined to $V_{dis}(R) + V_{ex}(R)$ starting at $R = 16 a_0$. The C_6 coefficient is taken from Ref. [37] and the C_8 and C_{10} coefficients are taken from Ref. [36]. The exchange potential is from Ref. [38] where the exchange parameters are $\alpha = 3.63$, $\beta = 1.512 1/a_0$, and $B = 0.27$ a.u., respectively.

V. VIBRATIONAL BOUND STATES AND SCATTERING LENGTH

In order to test the potentials constructed in the previous sections we numerically calculated the rovibrational bound states and compared them with the experimentally obtained term values of Ref. [17]. The eigenvalues of the Schrödinger equation for the ground state Hamiltonian have been obtained for each of the four (splined) adiabatic potentials shown in Figs. 1 and 2. The ground state Hamiltonian includes the electrostatic interaction in form of the $^1\Sigma_g^+$ Born-Oppenheimer potential, the mechanical rotation operator, $\hat{l}^2/2\mu R^2$, and the kinetic energy operator.

The experimental term values are relative to the $\nu = 0, J = l = 0$ bound state. Consequently, theoretical term values of a potential are defined relative to the energy of the $\nu = 0, J = 0$ level of this potential. Our difference measure Δ is given by the square root of the averaged squared difference between the theoretical and experimental term values. The difference averaged over 254 ($\nu = 0 - 12, J = l = 10 - 68$) rovibrational levels lying below the dissociation energy for four potentials is given in Table I. The table shows that the IPA potential is one order of magnitude better than the RKR potential in representing the experimental term values, confirming the predicted improvement by Ref. [18]. The MVB potential is about as accurate as the RKR potential while the potential of Ref. [30] is clearly the least accurate.

We have set up a quantum scattering calculation for two ground state Mg atoms. For ultra-cold atom physics the relevant properties of an interaction potential are the number of s-wave bound states and the scattering length a at zero collision energy. The number of bound states of a potential is equal to the number of nodes of the zero-energy scattering wavefunction. We find that the number of bound states is different for each of our four potentials. In fact, we have 18, 19, 18, and 20 bound states for the RKR-, IPA-, and MVB-potential, and the potential of Ref. [30], respectively. Qualitatively, this variation can be understood from the long-range shape of these four potentials. The dispersion potential of Ref. [30] is the most attractive of all four potentials consistent with the observation that it has the largest number of bound states. The difference in dissociation energy does not lead to a change in the number of bound states. Notice that $v=12$ is the most-weakly-bound experimentally observed s-wave vibrational level, that is, the last seven vibrational levels have not been observed.

For the remainder of the paper we restrict scattering calculations to the IPA potential, since the discrepancy with the experimental term values for the IPA potential is an order of magnitude better than that of the others. The short-range part of the IPA potential smoothly connects to the state-of-the-art long-range dispersion and exchange potential of Refs. [37,36,38] and thus gives added confidence in the potential.

The IPA potential is tabulated in Table II and when splined has a scattering length of $26 a_0$. The scattering length of a potential is defined by the phase of the wavefunction at zero collision energy. It depends on the binding energy of the most-weakly bound s-

wave vibrational level. In order to obtain the accuracy of the scattering length for the IPA potential we must determine the effect of small changes to the potential. The uncertainty in the dissociation energy, the long-range dispersion coefficients, and the shape of the short-range potential limit the accuracy of our determination. The allowed variations are chosen within the published uncertainties. The 1 cm^{-1} uncertainty of the dissociation energy of Ref. [18] leads to a $7 a_0$ uncertainty in a . The effects of the uncertainty in the dissociation energy was studied by uniformly shifting the IPA potential for $R < 14.5 a_0$, fitting smoothly to the dispersion potential.

The 12 a.u. uncertainty in the C_6 coefficient of Ref. [37] adds an additional $7 a_0$ uncertainty to a , while uncertainties in the C_8 and C_{10} coefficients add $1.4 a_0$ and $0.5 a_0$, respectively. These corrections to the potential do not change the agreement between the calculated and experimental bound state term values. Nevertheless, a Δ of 0.22 cm^{-1} does imply that the shape of potential is not fully characterized, which introduces additional uncertainties to the scattering length. Local changes to the potential on the order of Δ are needed. Since Δ is about six times smaller than the uncertainty in the dissociation energy we can estimate the additional uncertainty in a to be $1 a_0$. The largest contributions to the uncertainty in the scattering length are, therefore, due to the uncertainty in D_e and C_6 . None of the discussed uncertainties in the potential changes the number of bound states. The final value for the scattering length of the IPA potential is $26(10) a_0$ or $1.4(5) \text{ nm}$ by adding the uncertainties in quadrature. The potential has 19 s -wave bound states.

Figure 3 shows partial cross sections of two colliding ground state Mg atoms as a function of collision energy. The contributions of s -, d -, and g -wave collisions are shown. The partial-wave cross section is defined as

$$\sigma_l = (2l + 1) \frac{8\pi}{k^2} \sin^2 \delta_l(k) \quad (1)$$

where $\delta_l(k)$ is the ${}^1\Sigma_g^+$ phase shift for l -wave collisions and k is the relative wavenumber of the collision. The cross section is calculated for the potential which has $a=26 a_0$ and is tabulated in Table II. The s -wave cross section has a maximum at $E/k_B = 3 \text{ mK}$ and then decreases monotonically up to $E/k_B = 50 \text{ mK}$. At zero collision energy the s -wave cross section equals $8\pi a^2$. The d - and g -wave partial cross sections are zero at zero collision energy and then rise rapidly and have a maximum at much higher collision energy than that given by the height of the d - and g -wave centrifugal barrier. In fact, the centrifugal barriers are at $E/k_B = 7.8 \text{ mK}$ and 47 mK for the d - and g -wave, respectively.

In summary, we have constructed four ${}^1\Sigma_g^+$ potentials for the collision between two ground state Mg atoms. Two of these potentials are based on the experimentally determined term values of the dimer, while the other two were of a theoretical origin. The MVB theoretical potential is calculated in this Paper. By comparing the experimental term values with those calculated for the four Born-Oppenheimer potentials we conclude that the theoretical MVB potential is of similar accuracy as the “experimentally determined” RKR potential. Given the difficulty of introducing electron correlations into the molecule the agreement is remarkable. Existing long-range dispersion and exchange coefficients have been discussed as well.

The best ${}^1\Sigma_g^+$ potential is obtained from an IPA potential for $R < 14.5 a_0$ connected to a dispersion potential based on Refs. [37] and [36]. This potential reproduces the experimental term values to 0.2 cm^{-1} , an order of magnitude better than the comparison for the other three

potentials, and gives a scattering length of $+1.4(5)$ nm where the error is predominantly due to the uncertainty in D_e and the C_6 dispersion coefficient. A positive sign of the scattering length suggests that a Bose-Einstein condensate of ground state Mg atoms is stable.

REFERENCES

- [1] K. Sengstock, U. Sterr, G. Hennig, D. Bettermann, J.H. Muller and W. Ertmer, *Optics Communications* **103**, 73 (1993).
- [2] F. Ruschewitz, J. Peng, H. Henderthur, N. Scharreath, and W. Ertmer, *Phys. Rev. Lett.* **80**, 3173 (1998).
- [3] P.S. Julienne, F.H. Mies, E. Tiesinga and C.J. Williams, *Phys. Rev. Lett.* **78**, 1880 (1997).
- [4] E. A. Curtis, C. W. Oates, and L. Hollberg, *Phys. Rev. A* **64**, 031403 (2001); T. Binnewies, G. Wilpers, U. Sterr, F. Riehle, J. Helmcke, T.E. Mehlstäubler, E.M. Rasel, and W. Ertmer, *Phys. Rev. Lett.* **87**, 123002 (2001).
- [5] H. Katori, T. Ido, Y. Isoya, and M. Kuwata-Gonokami, *Phys. Rev. Lett.* **82**, 1116 (1999).
- [6] H. Katori, T. Ido, and M. Kuwata-Gonokami, *J. Phys. Soc. Japan* **68**, 2479 (1999).
- [7] T. Ido, Y. Isoya, and H. Katori, *Phys. Rev. A* **61**, 61403 (2000).
- [8] H. Katori, T. Ido, Y. Isoya, and M. Kuwata-Gonokami, *Atomic Physics 17*, Editors E. Arimondo, P. DeNatale, and M. Inguscio (AIP, 2001), pp. 382-396.
- [9] F. Riehle, P. Kersten, H. Schnatz, T. Trebst, G. Zinner, and J. Helmcke, *Laser Phys.* **8**, 664 (1998).
- [10] F. Riehle, H. Schnatz, B. Lipphardt, G. Zinner, T. Trebst, and J. Helmcke, *IEEE T Instrum. Meas.* **48**, 613 (1999).
- [11] C. W. Oates, F. Bondu, R. W. Fox, and L. Hollberg, *Eur. Phys. J. D* **7**, 449 (1999).
- [12] C.W. Oates, E.A. Curtis, and L. Hollberg, *Opt. Lett.* **25**, 1603 (2000).
- [13] Th. Udem, S.A. Diddams, K.R. Vogel, C.W. Oates, E.A. Curtis, W.D. Lee, W.M. Itano, R.E. Drullinger, J.C. Bergquist, and L. Hollberg, *Phys. Rev. Lett.* **86**, 4996 (2001).
- [14] G. Zinner, T. Binnewies, F. Riehle, and E. Tiemann, *Phys. Rev. Lett.* **85**, 2292 (2000).
- [15] M. Machholm, P. S. Julienne, and K.-A. Suominen, *Phys. Rev. A* **64**, 033425 (2001).
- [16] P.O. Fedichev, M.W. Reynolds, U.M. Rahmanov, and G.V. Shlyapnikov, *Phys. Rev. A* **53**, 1447 (1996); M.R. Doery, E.J.D. Vredenburg, S.S. Op de Beek, *Phys. Rev. A* **58**, 3673 (1998).
- [17] W. J. Balfour and A. E. Douglas, *Can. J. Phys.* **48**, 901 (1970).
- [18] C. R. Vidal and H. Scheingraber, *J. Mol. Spectrosc.* **65**, 46 (1977).
- [19] B. Liu and A. D. McLean, *J. Chem. Phys.* **59**, 4557 (1973).
- [20] P. Bertoncini and A. C. Wahl, *Phys. Rev. Lett.* **25**, 991 (1970); *ibid.*, *J. Chem. Phys.* **58**, 1259 (1973).
- [21] C. W. Muhlhausen and D. D. Konowalow, *Chem. Phys.* **7**, 143 (1975).
- [22] P. J. Hay and T. H. Dunning, *J. Chem. Phys.* **65**, 2679 (1976).
- [23] W. J. Stevens and M. Krauss, *J. Chem. Phys.* **67**, 1977 (1977).
- [24] G. D. Purvis and R. J. Bartlett, *J. Chem. Phys.* **68**, 2114 (1978).
- [25] G. H. F. Diercksen, V. Kello, and A. Sadlej, *Chem. Phys.* **103**, 55 (1986).
- [26] G. Chalasinski, D. J. Funk, J. Simons, and W. H. Breckenridge, *J. Chem. Phys.* **87**, 3569 (1987).
- [27] K. G. Dyall and A. D. McLean, *J. Chem. Phys.* **97**, 8424 (1992).
- [28] W. Klopper and J. Almløf, *J. Chem. Phys.* **90**, 5167 (1993).
- [29] F-M Tao and Y-K Pan, *Mol. Phys.* **81**, 507 (1994).

- [30] E. Czuchaj, M. Krosnicki and H. Stoll, submitted to *Theoretical Chemistry Accounts* (2001).
- [31] S. Kotochigova, E. Tiesinga, and I. Tupitsyn, in "New Trends in Quantum Systems in Chemistry and Physics", **1**, 219 (Kluwer Academic Publ., The Netherlands, 2001).
- [32] W. C. Stwalley, *Chem. Phys. Lett.* **7**, 600 (1970)
- [33] W. C. Stwalley, *J. Chem. Phys.* **54**, 4517 (1971).
- [34] K. C. Li and W. Stwalley, *J. Chem. Phys.* **59**, 4423 (1973).
- [35] J. F. Stanton, *Phys. Rev. A* **49**, 1698 (1994).
- [36] J. M. Standard and P. R. Certain, *J. Chem. Phys.* **83**, 3002 (1985).
- [37] S. G. Porsev and A. Derevianko, *Phys. Rev. A*, accepted November 2001.
- [38] A. A. Radzig and B. M. Smirnov, in "Reference Data on Atoms, Molecules, and Ions", part 9, 463, (Springer-Verlag, 1985).

FIGURES

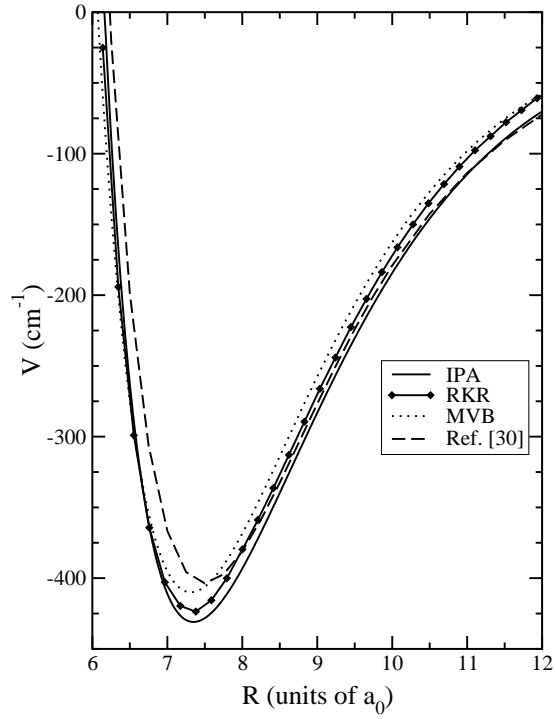


FIG. 1. Ground state $^1\Sigma_g^+$ potential energy curves obtained by different methods as a function of internuclear separation R . The internuclear separation is in units of $a_0 = 0.0529177$ nm. The solid line with filled diamonds corresponds to the RKR potential; the solid line shows the IPA potential; the dotted line is our MVB potential and the dashed line is the potential by Ref. [30]

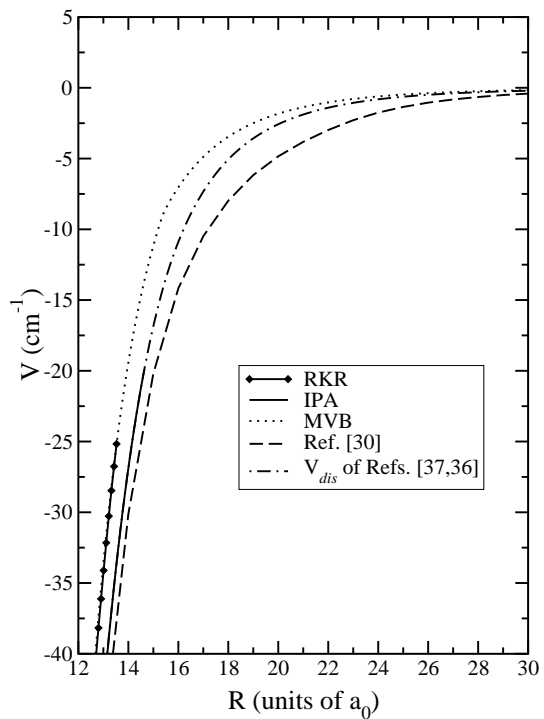


FIG. 2. $^1\Sigma_g^+$ potential energy curves as a function of internuclear separation. The region where the RKR and IPA potential are connected to the long-range dispersion potential is shown. The line style is the same as that used in Fig. 1 where in addition the dash-dotted line is the dispersion potential using the data from Refs. [37,36].

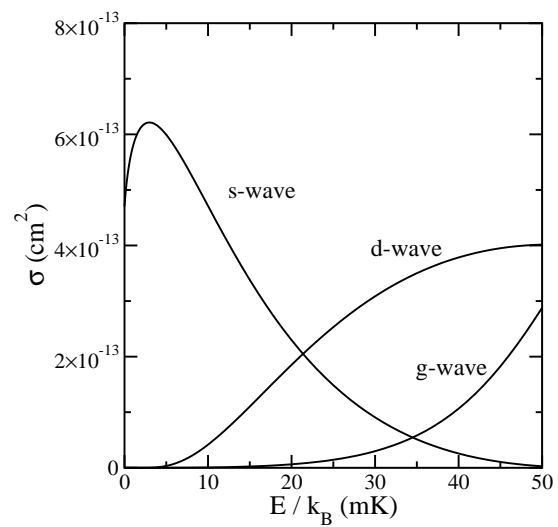


FIG. 3. The s , d , and g -wave cross-section of the ground state Mg + Mg collision as a function of collision energy.

TABLES

TABLE I. The square root of the averaged squared difference between four calculated Born-Oppenheimer potentials of the $X^1\Sigma_g^+$ state and measured rovibrational energies of Ref. [17].

Potential	Difference $\Delta(\text{cm}^{-1})$
RKR	2.1
IPA	0.2
<i>Ab initio</i> Ref. [30]	11.9
<i>Ab initio</i> this work	2.3

TABLE II. Constructed IPA potential for the $X^1\Sigma_g^+$ ground potential of Mg_2 . For $R > 18 a_0$ the analytical dispersion and exchange potential discussed in the text is used.

$R(a_0)$	$V(\text{cm}^{-1})$	$R(a_0)$	$V(\text{cm}^{-1})$
5.00	3684.419	8.50	-339.579
5.10	2989.552	8.70	-316.957
5.20	2409.684	8.90	-294.292
5.30	1925.473	9.10	-272.121
5.40	1520.991	9.30	-250.742
5.50	1183.093	9.50	-230.345
5.60	900.903	9.70	-211.057
5.70	665.394	9.90	-192.949
5.80	469.063	10.10	-176.055
5.90	305.652	10.30	-160.376
6.00	169.935	10.50	-145.892
6.10	57.539	10.70	-132.563
6.20	-39.100	10.90	-120.340
6.30	-130.963	11.10	-109.165
6.40	-204.311	11.30	-98.974
6.50	-262.877	11.50	-89.703
6.60	-309.439	11.70	-81.285
6.70	-346.071	11.90	-73.654
6.80	-374.322	12.10	-66.749
6.90	-395.542	12.30	-60.505
7.00	-411.247	12.50	-54.867
7.06	-418.550	12.70	-49.782
7.14	-425.235	12.90	-45.205
7.22	-428.791	13.10	-41.098
7.30	-430.650	13.30	-37.398
7.36	-430.956	13.50	-34.043
7.44	-429.909	13.70	-30.982
7.50	-428.008	13.90	-28.190
7.56	-425.243	14.10	-25.649
7.62	-421.888	14.30	-23.341
7.68	-418.145	14.50	-21.248
7.74	-414.151	15.00	-16.855
7.80	-410.024	15.50	-13.472
7.86	-405.861	16.00	-10.896
7.92	-401.352	16.50	-8.910
7.98	-396.181	17.00	-7.334
8.10	-384.374	17.50	-6.075
8.30	-362.286	18.00	-5.062